# The structure of LepA, the ribosomal back translocase

**Robin N. Evans***, **Gregor Blaha***, **Scott Bailey***†, **and Thomas A. Steitz***†‡§

Departments of *Molecular Biophysics and Biochemistry and ‡Chemistry and †Howard Hughes Medical Institute, Yale University, New Haven, CT 06520-8114

Contributed by Thomas A. Steitz, February 8, 2008 (sent for review January 24, 2008)

**LepA is a highly conserved elongation factor that promotes the back translocation of tRNAs on the ribosome during the elongation cycle. We have determined the crystal structure of LepA from *Escherichia coli* at 2.8-Å resolution. The high degree of sequence identity between LepA and EF-G is reflected in the structural similarity between the individual homologous domains of LepA and EF-G. However, the orientation of domains III and V in LepA differs from their orientations in EF-G. LepA also contains a C-terminal domain (CTD) not found in EF-G that has a previously unobserved protein fold. The high structural similarity between LepA and EF-G enabled us to derive a homology model for LepA bound to the ribosome using a 7.3-Å cryo-EM structure of a complex between EF-G and the 70S ribosome. In this model, the very electrostatically positive CTD of LepA is placed in the direct vicinity of the A site of the large ribosomal subunit, suggesting a possible interaction between the CTD and the back translocated tRNA or 23S rRNA.**

back translocation | crystal structure | ribosome | elongation factor

The *lepA* gene was discovered as the leading ORF of the bicistronic lep operon of the signal peptase I in *Escherichia coli* (1, 2). LepA is highly conserved in eubacteria, chloroplasts, and mitochondria (3, 4) and exhibits considerable similarity to GTPases involved in translation (5). The involvement of LepA in translation was confirmed by photo cross-linking a ribosome bound oxazolidone antibiotic to LepA (6).

An analysis of all of the translational GTPase genes of 191 fully sequenced bacterial genomes revealed the presence of at least one LepA-coding gene in every bacterial genome, with the exception of one of the sequenced strains of *Streptococcus pyogenes* (7). Although the near-universal presence of LepA implies an important role in bacteria, LepA knockout strains of *E. coli* (8) and *Staphylococcus aureus* (6) are viable, however, this does not exclude the possibility that LepA is essential under certain growth conditions, as seen in *Helicobacter pylori* for which LepA is essential to sustain the growth at low pH (9).

Although functions were hypothesized earlier (5, 9–11), Nierhaus and colleagues (3) finally deduced the unique function of LepA in protein synthesis through biochemical studies of the interaction of LepA with the ribosome. During protein synthesis, a unidirectional sequence of reactions elongates the nascent chain successively by 1 amino acid (aa) at a time. This so-called elongation cycle begins with an mRNA-dependent recognition of an amino-acylated tRNA, which is delivered to the ribosome by EF-Tu in complex with GTP. The hydrolysis of the EF-Tu bound GTP induces the accommodation of amino-acylated tRNA into the A site and leads to the dissociation of EF-Tu/GDP from the ribosome. After full accommodation of the delivered amino-acylated tRNA into the A site, the peptidyl residue attached to the adjacent P site tRNA is transferred onto the aminoacylated tRNA, thereby elongating the nascent chain by 1 aa. To enable another round of peptide elongation, the complex of mRNA, deacylated tRNA in the P site, and a peptidyl-tRNA in the A site is translocated by precisely one codon, thus positioning the peptidyl-tRNA in the P site, a deacylated tRNA in the E site, and the next codon of the mRNA in the A site. This transition from a pre- to a posttranslocational state is promoted by EF-G via GTP hydrolysis. LepA promotes the reversal of this step. Upon binding to the posttranslocational state, it promotes the back translocation of the mRNA–tRNA complex to the pretranslocational state. Given its unique function in translation and high sequence conservation in bacteria, it was suggested to rename LepA to elongation factor 4 (EF4). *In vivo*, LepA might increase the fidelity of translation by back-translocating ribosomes from faulty translocation reactions, thus giving EF-G a second chance for correct translocation (3).

Here, we present the 2.8-Å-resolution crystal structure of LepA from *E. coli*, which was solved by heavy atom isomorphous replacement and noncrystallographic symmetry averaging. The high structural similarity of the individual domains to their homologous domains of EF-G enabled us to derive a homology model for LepA from an EF-G bound 70S cryo-EM structure and shed light onto the possible mechanism of back translocation.

## Results and Discussion

**Structure Determination and Domain Organization.** LepA crystallizes in the $P2_1$ space group with six copies in the asymmetric unit, which are arranged in three sets of dimers along a 3-fold screw axis that is almost perpendicular to the crystallographic 2-fold screw axis. There is an intermolecular disulfide link between two Cys-552 residues that lie at the tip of the C-terminal domain (CTD). This disulfide bond is positioned directly on the 2-fold axis relating to each dimer and is most likely the result of crystal packing because LepA appears to be a monomer in solution under reducing conditions as shown by gel filtration (data not shown).

Despite its high sequence similarity to EF-G, repeated attempts to solve the structure of LepA by molecular replacement using the 2.8-Å-resolution native dataset were presumably hindered by the high noncrystallographic symmetry (NCS). After extensive screening for a heavy-atom derivative, only one 6-Å dataset from a crystal soaked in samarium acetate was isomorphous enough to yield an initial phase set that was calculated by combining the single isomorphous replacement and anomalous scattering phase information. The initial phases were dramatically improved by multidomain noncrystallographic symmetry averaging of the six NCS symmetry mates, which resulted in an interpretable electron-density map (Fig. 1*B* and *C*). The structure of one monomer, molecule A of LepA, was built manually by using Coot (12). The other five monomers (B–F) were generated initially by applying the NCS symmetry operators to fitted molecule A and are nearly identical after refinement (RMSD values range from 0.31 to 0.55 Å).Successive rounds of building and refinement resulted in a final $R_{\text{free}}$ of 29.6% and $R_{\text{factor}}$ of 25.2%.

---

Author contributions: R.N.E., G.B. and T.A.S. designed research; R.N.E., G.B. and S.B. performed research; R.N.E., G.B., and T.A.S. analyzed data; and R.N.E., G.B., and T.A.S. wrote the paper.

The authors declare no conflict of interest.

Freely available online through the PNAS open access option.

Data deposition: The atomic coordinates have been deposited in the Protein Data Bank, www.pdb.org (PDB ID code 3CB4).

[§] To whom correspondence should be addressed. E-mail: peggy.eatherton@yale.edu.

This article contains supporting information online at www.pnas.org/cgi/content/full/0801308105/DCSupplemental.

© 2008 by The National Academy of Sciences of the USA

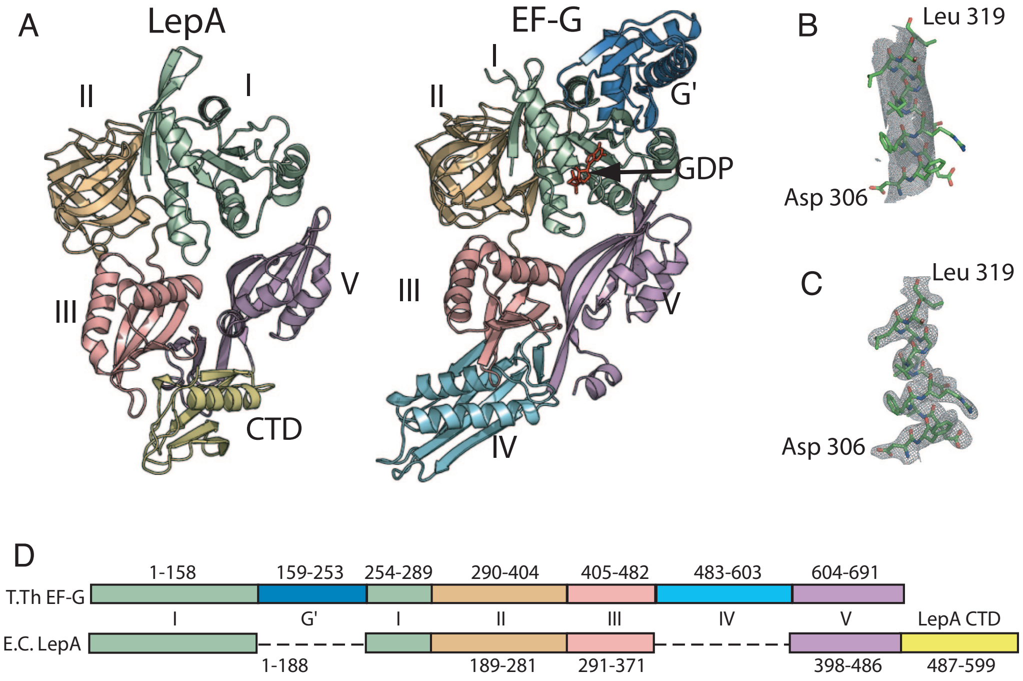

**Fig. 1.** Crystal structure of LepA. (*A*) Ribbon representations of the structures of LepA (*Left*) and EF-G (*Right*). The EF-G coordinates [PDB ID code 1FNM (14)] correspond to the crystal structure of a His573Ala mutant bound to GDP (red). The homologous domains between the two are colored the same, I (green), II (light orange), III (pink), and V (purple). G′ and IV of EF-G are colored blue and cyan, whereas the CTD of LepA is colored yellow. (*B*) The experimentally phased electron density map of a representative helix in domain III calculated at 6-Å resolution and contoured at 1.2 $\sigma$. (*C*) The 6-fold NCS-averaged electron-density map at 2.8-Å resolution contoured at 1.2 $\sigma$ shows the same representative helix from domain III with a dramatic improvement in the quality and the resolution of its electron density. (*D*) Alignment of *T. thermophilus* EF-G and *E. coli* LepA sequences with their domains indicated as boxes and color coded as described above. The important domain differences are the absence of domains IV and G′ in LepA and the addition of a unique CTD.

Each monomer of LepA can be subdivided into five domains based on the domain definition of EF-G (Fig. 1 *A*and *D*). LepA has no domain that is homologous to domain IV of EF-G, and therefore we chose to name the fourth domain of LepA domain V because of its homology to domain V of EF-G. Domain I, which spans residues 1–188, contains the consensus GTPase fold and consists of six $\beta$-strands surrounded by four $\alpha$-helices and constitutes the characteristic G domain found in translational GTPases (13). Domain II (residues 189–281) is composed entirely of $\beta$-sheets and has a distinctive OB-fold (oligonucleotide/oligosaccharide binding).

Domains III (residues 291–371) and V (residues 398–486) both have the same double-split $\beta$-$\alpha$-$\beta$ fold (14). After domain V, is the unique CTD of LepA (residues 487–595). The part of the CTD that has been modeled is composed of one long $\alpha$-helix that is cradled by four short strands of a $\beta$-sheet. The final 44 aa were not visible in the electron-density map and are therefore not included in the model. Like EF-G, the domains of LepA seem to group together into two larger structures, the first of which is formed by domains I and II and the other by domains III and V plus the CTD.

**Comparison of LepA with EF-G Structures.** The structure of LepA closely resembles the known structures of EF-G, as was expected from their high degree of sequence similarity (Fig. 1*A*). The homologous domains I and II of both EF-G and LepA superimpose well onto each other with an RMSD of 1.58 Å for 238 C$\alpha$ atoms (Fig. 2*B*). One striking difference between domain I in LepA and in EF-G is the absence of the G′ domain in LepA. The functional role of the G′ domain of EF-G is unclear, however, cryo EM studies show that it forms an arc-like structure with the C-terminal domain of L7 at the base of the L7/L12 stalk (15). It was thought that the G′ domain of EF-G was involved in nucleotide exchange (13); however, this seems unlikely because LepA displays uncoupled ribosome-dependent GTPase activity similar to EF-G (3). Aside from the absence of the G′ domain, the only other difference in domain I is an extended loop between residues 64–70 in LepA, which corresponds to residues 74–76 in EF-G.

Domain II of LepA is missing the first two $\beta$-strands of the corresponding domain in EF-G. Interestingly, these two strands are also missing from EF-Tu (16). Other than the absence of the first two $\beta$-strands, the only other minor differences are the orientations of two loops. The loops between LepA residues 200–206 (EF-G 318–324) and residues 259–271 (EF-G 378–386) are all shifted ≈4 Å away from the homologous loops in EF-G.

Individually, domains III and V superimpose well onto the analogous domains of EF-G (domain III RMSD = 1.22 Å for 70 C$\alpha$ atoms, domain V RMSD = 1.38 Å for 80 C$\alpha$ atoms) (Fig. 2*B*). However, the orientations of these domains with respect to their G domains are different (Fig. 2*A*). Both domains III and V have the same double-split $\beta$-$\alpha$-$\beta$ fold seen in EF-G. This fold is often referred to as the RNA recognition motif and is found in many ribosomal proteins (14). The only major difference between the domain-III structures of these two factors is a 15-Å movement of the loop between residues 330–336 (EF-G 442–448). If this loop were in the same orientation in LepA as in EF-G, it would clash with the CTD. In EF-G, domains III and V are connected through domain IV, which is absent in LepA. Domains III and V of LepA are connected by two $\beta$-strands that bear a slight resemblance to the top of domain IV in EF-G.

**The Unique LepA C-Terminal Domain.** The most interesting part of the LepA structure is its CTD, because it is not homologous to any region in EF-G. A search for structural homologues of the CTD submitted to the DALI server (www.ebi.ac.uk/dali/) re-

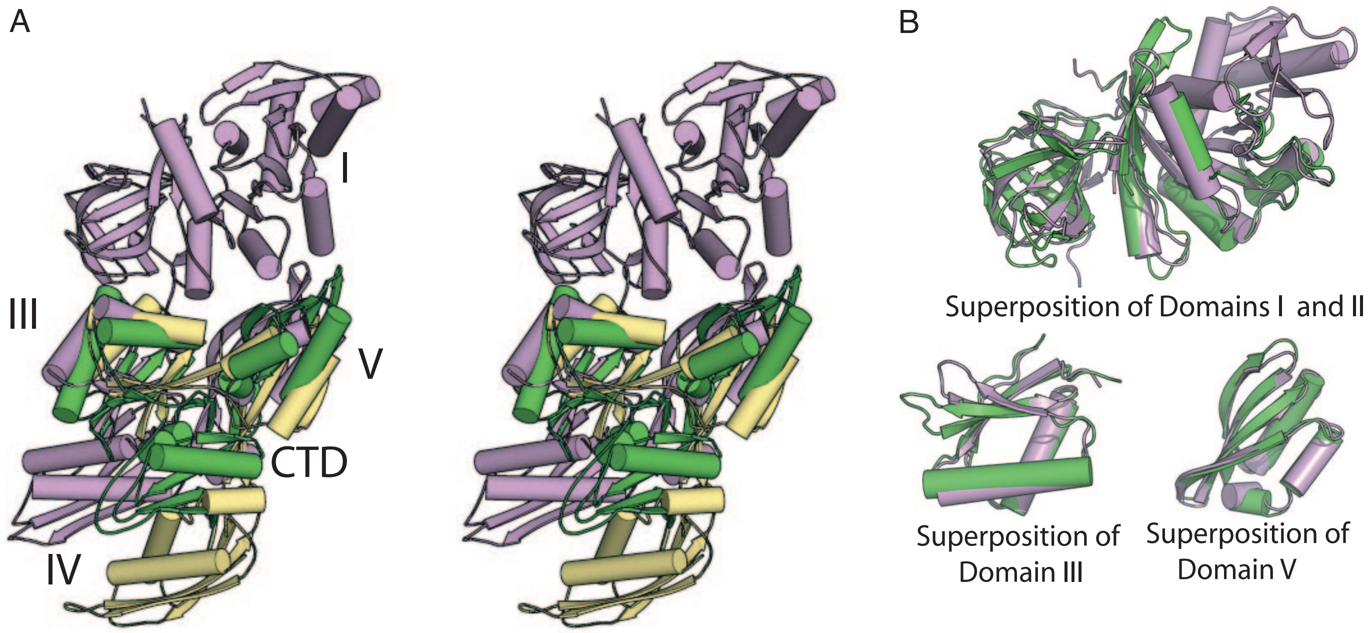
A
I
III
V
CTD
IV
B
Superposition of Domains I and II
Superposition of Domain III
Superposition of Domain V

**Fig. 2.** Comparison of LepA with EF-G. (*A*) Stereoview of the superposition of LepA (green), H573A mutant EF-G (purple), and EF-G (light orange) bound to the 70S ribosome from the 7.3-Å electron microscopy reconstruction (coordinates provided by Christian Spahn). All three are oriented by superimposing their domains I and II. For legibility, domains I and II of LepA and EF-G bound to the 70S are omitted. (*B*) Superposition of the individual domains of LepA (green) and EF-G (purple).

turned no hits with a $Z$-score $>3$, which is indicative of a novel fold. The CTD is connected to the terminal long $\beta$-strand of domain V (Fig. 1*A*). The first $\beta$-strand of the CTD is followed by a long loop, which forms an interface with domain III, and a second short $\beta$-strand. This $\beta$-strand leads into a long $\alpha$-helix, which was the only portion of the CTD visible in the electron density before 6-fold NCS averaging. After the helix are two antiparallel $\beta$-strands and a long loop. Unfortunately, no electron density was visible past residue Gly 555, thus the last 44 aa of the CTD are not included in the model. The CTD contains numerous positively charged residues (27 in *E. coli*), many of which are quite conserved among different LepA homologues (supporting information (SI) Fig. S1*D*). The entire CTD of *E. coli* LepA is very basic and has a net predicted charge of approximately $+13$ at physiological pH, which may function to facilitate the interaction of LepA with RNA (Fig. 3*D*).

**The Nucleotide-Binding Pocket.** The nucleotide-binding site is empty in the structure of LepA despite our attempts to cocrystallize LepA with either guanosine di- or triphosphate or to soak the nucleotides into the crystals. The high $Mg^{2+}$ concentration necessary for improving the diffraction quality of the crystals might have reduced the free concentration of the nucleotides below the dissociation constant for its binding to LepA. The electron density in the P-loop region of all six LepA copies is weak, and therefore, because the structure between Val-13 and Ser-18 could not be built with confidence, they were omitted form the model. The residues in this region of the P loop are well conserved between EF-G and LepA, with the exception of His-15 (Ala-23 in *Thermus thermophilus* EF-G). However, this histidine is conserved in EF-Tu (Fig. S1 *A–C*). The nucleotide and the missing residues from the P loop can be easily modeled into the active site by superimposing the G domain of EF-G (or EF-Tu) onto LepA (Fig. S1*B*). The switch I region of LepA (residues 29–57) is also disordered in our structure, which is not surprising, given that it is also disordered in most crystal structures of EF-G and is thought to be highly flexible, and becomes ordered only upon nucleotide binding (17).

**Orientation of Domains III and V.** The crystal structures of unliganded EF-G and its complex with GDP are nearly identical (17, 18). The flexibility of EF-G was first revealed from a comparison of the wild-type crystal structures with a crystal structure of GDP bound to EF-G containing a H537A mutation at the tip of domain IV (which does not hinder translocation). When the mutant structure was compared with the wild-type structures of EF-G, it was discovered that domains III, IV, and V rotate significantly with respect to domains I and II (14, 17). A reorientation of domain III relative to domains IV and V has been observed in the recently published crystal structure of GTP-bound EF-G-2 (an EF-G homologue protein from *T. thermophilus*). These rearrangements result in a 20-Å displacement of the tip of domain IV compared with the *apo* structure of EF-G (19). Similarly, large-scale conformational changes were detected in cryo EM studies of EF-G bound to the ribosome (19–25), in which the domain rearrangements result in domain IV moving into the A site.

When domains I and II of LepA are aligned onto domains I and II of EF-G, the orientations of domains III and V in LepA are different from domains III and V of the various structures of EF-G (Fig. 2*A*). This reinforces the idea that the domain positions are very flexible and are capable of undergoing large conformational changes, perhaps upon binding of nucleotide or binding to the ribosome. Comparison of the H537A mutant crystal structure of EF-G with that of LepA shows that domain III rotated by $\approx$10°. This rotation is not quite as large as the rotation of domain III observed in the EM models of the EF-G bound to the ribosome. Domain V, on the other hand, when compared with the H573A mutant undergoes a more significant reorientation. The domain V of LepA is rotated $\approx$10° and translated $\approx$15 Å away from domain V of the H573A mutant of EF-G. This allows domains V and I of LepA to form an interface, which has not been observed in structures of EF-G.

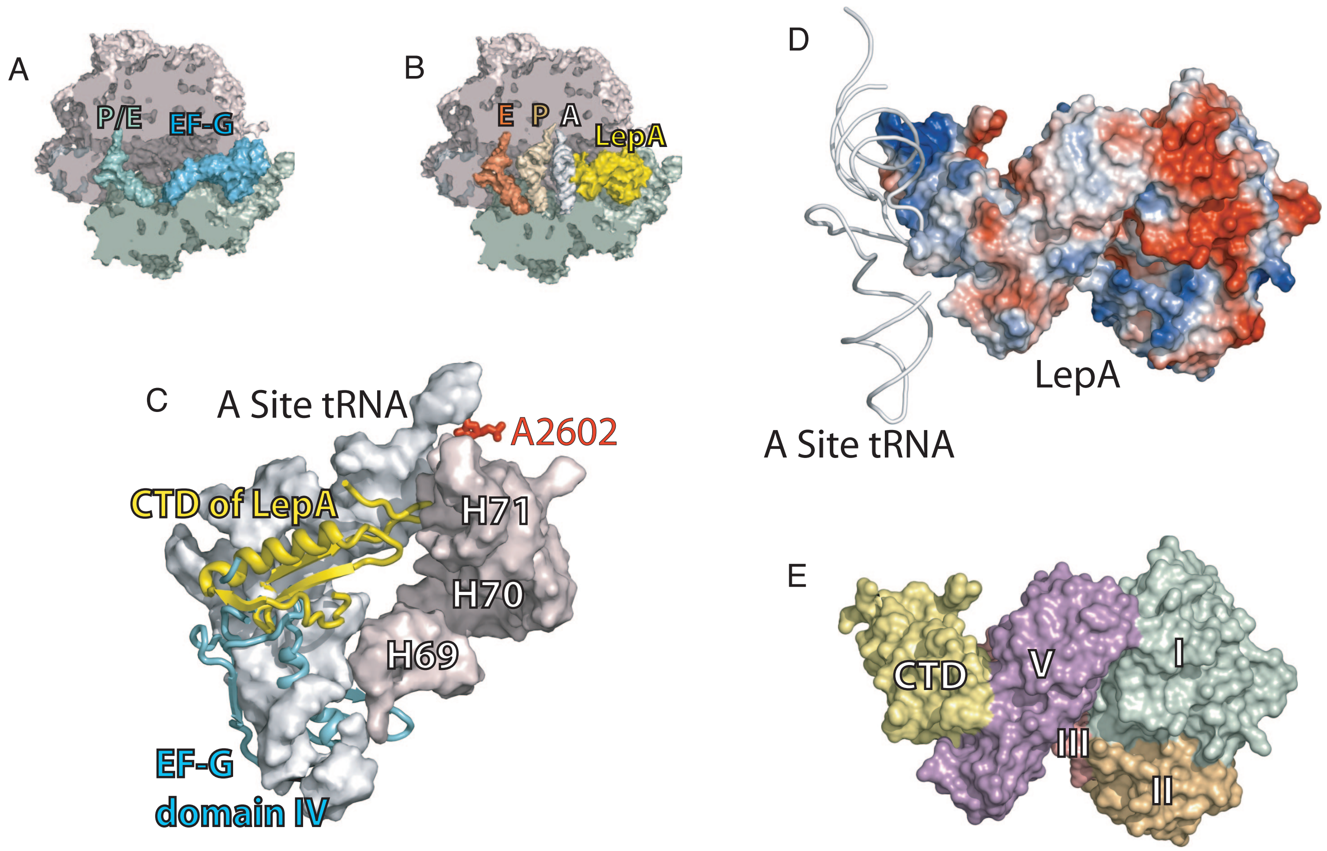

**Fig. 3.** Homology model for LepA bound to the 70S ribosome. (*A*) The 7.3-Å-resolution electron microscopy structure of EF-G (cyan) bound to the 70S ribosome that contains a deacylated tRNA in the P/E site (aquamarine) (19). The large ribosomal subunit is represented in light pink and the small in light green. (*B*) Homology model derived from the 7.3-Å-resolution EM structure in *A* by superpositioning the domains I and II of LepA onto the corresponding domains of EF-G and by aligning the tRNAs from the *T. thermophilus* 70S ribosome via superposition the large subunits [PDB IDs 1GIX and 1GIY (42)]. LepA is displayed in yellow; the A site, P site, and E site tRNA are displayed in alice blue, khaki, and orange, respectively. (*C*) Close up view of the A site of the ribosome showing the positioning of the CTD of LepA (yellow ribbons) in close proximity to the CCA end of the A-site tRNA and several helices of the 23S rRNA in the A site (light pink). In addition residue A2602 (red), which seems to be in close proximity to bound LepA (6) is displayed. (*D*) The electrostatic complimentarity of CTD of LepA to A-site tRNA as observed in the homology model of LepA binding to the ribosome. Positively charged surface patches are displayed in blue, and negatively charged surface patches are displayed in red. (*E*) Surface representation of LepA with the domains color coded as described in the Fig. 1 legend.

**Homology Model of LepA Bound to the 70S Ribosome.** Despite a wealth of biochemical and structural data, the mechanism of forward translocation of tRNAs on the ribosome facilitated by EF-G has not been completely elucidated. Models for translocation suggest that EF-G bound to GTP undergoes a GTPase-activated rearrangement upon binding to the ribosome. After GTP hydrolysis, a rate limiting conformational change unlocks the ribosome (26–28) allowing the tRNA-mRNA complex to sample both pre- and posttranslational states. The directionality of the translation seems to be controlled by domain IV invading the empty A site of the forward-translocated tRNA–mRNA-complex and thereby forming a barrier for reverse translocation (19, 29). Cryo-EM studies observe ratcheting of the ribosomal subunits upon formation of ribosome complexes with EF-G stalled with bound nonhydrolyzable GTP (19, 20, 23). This ratchet motion occurs before the GTPase-induced unlocking of the ribosome along the reaction pathway of translocation (22, 30). Because, this ratcheting motion of the subunits is required for translocation (31) and given the high structural similarity between EF-G and LepA, it seems plausible that binding of LepA induces ratcheting and unlocking of ribosomes in an EF-G-like manner (11). Therefore, we chose the high resolution cryo-EM reconstruction of EF-G bound to the ribosome, which was stalled with a nonhydrolyzable GTP analogue (19) as a starting model for our homology modeling. In our first model, we superimposed domains I and II of LepA onto the corresponding domains of EF-G bound to the ribosome. The high degree of sequence identity and structural similarity of domains I and II between LepA and EF-G supports the assumption that they occupy the same binding site on the ribosome (Fig. 3 *A* and *B*). Because EF-G undergoes conformational changes upon binding to the ribosome, one could assume that LepA undergoes similar domain rearrangements. To examine these possible domain rearrangements, we generated another homology model by superimposing the domain V of LepA onto the equivalent domain of EF-G. Both approaches produced homology models that place the CTD of LepA in approximately the same location on the ribosome, although in different orientations. Interestingly, the CTD seems to be in close proximity to the A site of the 50S subunit, in sharp contrast to the EF-G-specific domain IV, which reaches down into the A site of the 30S subunit. In our homology models of LepA binding to the ribosome, the CTD appears to be close to the 23S rRNA residues 1944–1948 and 2559–2562. These residues are in the A site near the CCA end of the tRNA bound in the A site of the *T. thermophilus* 70S ribosome crystal structure with a full-length tRNA (Fig. 3 *A–D*) (32). The close proximity of LepA to the CCA end of the A-site tRNA is consistent with *in vivo* photo cross-linking data that indicate a close proximity of LepA to A-2602, a residue in the peptidyltransferase center of the large ribosomal subunit (6).

**The Reverse Translocation of tRNAs.** The CTD of LepA may play a primary role in back translocation by providing additional binding interactions with a back-translocated tRNA. Because EF-G mutants lacking domain IV can still promote forward translocation (25, 33), the back-translocational activity of LepA cannot be explained by the absence of domain IV in LepA. We therefore expect that the LepA-specific CTD plays a major role in facilitating reverse translocation. Our homology model of LepA bound to the ribosome places this unique CTD in the vicinity of the A site of the large ribosomal subunit. The highly positive electrostatic charge of the CTD suggests that the CTD might interact with the A-site tRNA, perhaps with the CCA terminus (Fig. 3*D*). This interaction might stabilize the tRNA positioned in the A site and thereby shift the equilibrium between pre- and posttranslocational state toward the pretranslocational state. The stabilization of the CCA terminus in the A site of the large ribosomal subunit has been reported to inhibit translocation induced by sparsomycin and reduce translocation promoted by EF-G (34). Also to be considered is the possibility that the CTD interacts with the 23S ribosomal RNA and in some manner causes a change in the ribosome structure that favors the pretranslocation state (Fig. 3*C*).

We therefore propose the following model for reverse translocation. LepA preferentially binds to ribosomes in the posttranslocation state (3), a preference that might depend on the absence of the G′ domain. As is known to occur with EF-G, the binding of LepA might induce a ratcheting rotational motion of the subunits, followed by GTP hydrolysis and "unlocking" of the ribosome. The interactions between the CTD of LepA and the back translocated tRNA and/or possibly the 23S rRNA energetically favors the equilibrium of the ribosome toward the pretranslocation state, thereby causing the mRNA-tRNA complex to move backwards.

**Table 1. Data collection, phasing, and refinement statistics**

| | LepA |
|---|---|
| Space group | $P2_1$ |
| Unit cell dimensions | |
| *a*, *b*, *c*, Å | 97.96, 146.23, 139.31 |
| $\alpha$, $\beta$, $\gamma$, ° | 90, 100.6, 90 |
| Resolution, Å | 50–2.8 |
| $R_{\text{merge}}$[*,†], % | 11.7 (58.8) |
| $I/\sigma$[†] | 9.8 (1.4) |
| Completeness[†], % | 94.6 (64.9) |
| Redundancy[†] | 3.3 (2.4) |
| $R_{\text{cryst}}$[†,‡], % | 25.2 (41.1) |
| $R_{\text{free}}$[†,‡], % | 29.6 (44.2) |
| RMSD bond length, Å | 0.007 |
| RMSD bond angle, ° | 1.085 |
| Phasing power[†,§] | |
| Acentric (samarium acetate) | 1.96 (2.13) |
| Centric (samarium acetate) | 1.35 (1.28) |
| Figure of merit (samarium acetate) | 0.51 (0.38) |

[*] $R_{\text{merge}}$ is $\Sigma|I_j - \langle I\rangle|/\Sigma I$, where $I_j$ is the intensity of an individual reflection, and $I$ is the mean intensity for multiply recorded reflections.

[†] The values in parentheses are for the highest-resolution shell.

[‡] $R_{\text{cryst}}$ is $\|F_o - F_c\|/F_o$, where $F_o$ is an observed amplitude and $F_c$ a calculated amplitude; $R_{\text{free}}$ is the same statistic calculated over a subset of the data that has not been used for refinement.

[§] Phasing power is the RMS isomorphous difference divided by the RMS lack of closure.

## Materials and Methods

**General.** All chemicals except for those noted were purchased from Sigma–Aldrich. The genomic DNA of *E. coli* K12 was obtained from the American Type Culture Collection, oligonucleotides were obtained from Integrated DNA Technologies, and DNA sequencing was performed at the Keck Foundation Research Biotechnology Laboratory (Yale University).

**Construction of LepA Overexpression Clone and Purification of LepA.** The entire *lepA* gene was PCR amplified from the genomic DNA of *E. coli* K12 with primers that introduced upstream NcoI and downstream BamHI restriction sites for directional cloning into the pET28a vector (Novagene). *E. coli* BL21(DE3) cells (Stratagene) transformed with the pET28a lepA construct were grown at 37°C in LB medium, in the presence of 30 mg/liter kanamycin to an absorbance at 600 nm of 0.6 before induction with 1 mM isopropyl-$\beta$-D-thiogalactopyranoside(IPTG). Cells were grown for an additional 4 h before harvest. The harvested cells were lysed and clarified by ultracentrifugation, before loading onto a HisTrap HP column(GE Heathcare). Although LepA did not interact with the Ni Sepharose, this step was essential for crystallization. The HisTrap flowthrough was loaded onto a HiTrap Q FF ion-exchange column (GE Heathcare), and LepA was eluted off over a linear gradient to 1 M NaCl. The fractions containing LepA were combined, brought to a final concentration of 1 M ammonium sulfate, and loaded onto a phenyl Sepharose column (GE Heathcare). After a reverse ammonium sulfate gradient (1 to 0 M) the LepA-containing fractions were combined, concentrated, and loaded onto a HiLoad 26/60 Superdex 200 column (GE Heathcare) equilibrated in 50 mM Tris (pH 7.6) 10 mM $MgCl_2$, 50 mM $NH_4Cl$, and 2 mM DTT. The purified LepA fractions from the gel-filtration column were pooled and concentrated by ultrafiltration to 30 mg/ml as determined by the Bradford assay (Bio-Rad), using BSA as a standard. LepA was flash-frozen in liquid nitrogen in small aliquots and stored at −80°C until further use in crystallization experiments.

**Crystallization.** Thin needles of LepA were initially grown by vapor diffusion from a 2:1 ratio of 15 mg/ml LepA to well solution (100 mM Tris·HCl in a pH range of 8.00–8.75 and PEG 2000 MME in a range of 5–10%) within 2 weeks. Crystals grew within 2 days when 100 mM $MgCl_2$ was included in the well solution. Crystal quality was further enhanced by micro seeding, yielding crystals with dimensions of up to 400 × 50 × 50 $\mu$m. Crystals were stabilized by slowly increasing the concentration of PEG 2000 MME to a final concentration of 35% before flash-freezing in liquid propane.

**Structure Solution and Refinement.** Diffraction data were collected at 100 K at the beam line stations X-29 and X-25 at Brookhaven National Laboratory (Upton, NY), 24ID at the Argonne Photon Source (Argonne, IL), or 8.2.1 and 8.2.2 at the Advanced Light Source (Berkeley, CA). The raw data were processed and scaled with the HKL2000 program suite (35). General handling of scaled data was done in CCP4 (36). An isomorphous heavy-atom derivative was obtained by soaking stabilized crystals in cryoprotectant supplemented with 1 mM samarium acetate for 2 h before freezing. Heavy-atom sites were found by using ShelxD (37), and the initial phase set was calculated in SOLVE (38) by using single isomorphous replacement with anomalous scattering. Phases were further improved by 6-fold NCS averaging and extended to a resolution of 2.8 Å with Dmmulti (36). The structure was built in iterative cycles of model building in COOT (12) and refinement in REFMAC without NCS restraints (39) to a final $R_{\text{free}}$ of 29.6 and $R_{\text{factor}}$ of 25.2% (Table 1). Figures were generated with Pymol (40). The structure factors of our free *R* test set were randomly selected before the model was built. Because of the 6-fold NCS in the asymmetric unit the test set for the free *R* is not completely independent of the working *R* set (41). Calculating a truly independent free *R* would be challenging and would require us to start over from the diffraction data. Because of the quality of the experimental electron density map after NCS averaging, no significant changes in the overall structure are expected.

**ACKNOWLEDGMENTS.** We thank the staff at the beam line stations X-29 and X-25 at Brookhaven National Laboratory, 24ID at Advanced Photon Source , and 8.2.1 and 8.2.2 at Advanced Light Source for help during data collection and Christian Spahn for providing the coordinates of the EF-G complex with the ribosome derived from their cryo-EM reconstruction. This work was funded by National Institutes of Health Grant POL GM022778 (to T.A.S.).

1. March PE, Inouye M (1985) Characterization of the lep operon of *Escherichia coli*. Identification of the promoter and the gene upstream of the signal peptidase I gene. *J Biol Chem* 260:7206–7213.
2. Date T, Wickner W (1981) Isolation of the *Escherichia coli* leader peptidase gene and effects of leader peptidase overproduction *in vivo*. *Proc Natl Acad Sci USA* 78:6106–6110.
3. Qin Y, *et al.* (2006) The highly conserved LepA is a ribosomal elongation factor that back-translocates the ribosome. *Cell* 127:721–733.
4. Caldon CE, Yoong P, March PE (2001) Evolution of a molecular switch: Universal bacterial GTPases regulate ribosome function. *Mol Microbiol* 41:289–297.
5. March PE, Inouye M (1985) GTP-binding membrane protein of *Escherichia coli* with sequence homology to initiation factor 2 and elongation factors Tu and G. *Proc Natl Acad Sci USA* 82:7500–7504.
6. Colca JR, *et al.* (2003) Cross-linking in the living cell locates the site of action of oxazolidinone antibiotics. *J Biol Chem* 278:21972–21979.

7. Margus T, Remm M, Tenson T (2007) Phylogenetic distribution of translational GTPases in bacteria. *BMC Genomics* 8:15.
8. Dibb NJ, Wolfe PB (1986) lep operon proximal gene is not required for growth or secretion by *Escherichia coli*. *J Bacteriol* 166:83–87.
9. Bijlsma JJ, Lie ALM, Nootenboom IC, Vandenbroucke-Grauls CM, Kusters JG (2000) Identification of loci essential for the growth of *Helicobacter pylori* under acidic conditions. *J Infect Dis* 182:1566–1569.
10. March PE (1992) Membrane-associated GTPases in bacteria. *Mol Microbiol* 6:1253–1257.
11. Youngman EM, Green R (2007) Ribosomal translocation: LepA does it backwards. *Curr Biol* 17:R136–R139.
12. Emsley P, Cowtan K (2004) Coot: Model-building tools for molecular graphics. *Acta Crystallogr D* 60:2126–2132.
13. Liljas A, *et al.* (1995) Crystallographic studies of elongation factor G. *Biochem Cell Biol* 73:1209–1216.
14. Laurberg M, *et al.* (2000) Structure of a mutant EF-G reveals domain III and possibly the fusidic acid binding site. *J Mol Biol* 303:593–603.
15. Datta PP, Sharma MR, Qi L, Frank J, Agrawal RK (2005) Interaction of the G′ domain of elongation factor G and the C-terminal domain of ribosomal protein L7/L12 during translocation as revealed by cryo-EM. *Mol Cell* 20:723–731.
16. Nissen P, *et al.* (1995) Crystal structure of the ternary complex of Phe-tRNAPhe, EF-Tu, and a GTP analog. *Science* 270:1464–1472.
17. Czworkowski J, Wang J, Steitz TA, Moore PB (1994) The crystal structure of elongation factor G complexed with GDP, at 2.7 A resolution. *EMBO J* 13:3661–3668.
18. AEvarsson A, *et al.* (1994) Three-dimensional structure of the ribosomal translocase: elongation factor G from *Thermus thermophilus*. *EMBO J* 13:3669–3677.
19. Connell SR, *et al.* (2007) Structural basis for interaction of the ribosome with the switch regions of GTP-bound elongation factors. *Mol Cell* 25:751–764.
20. Agrawal RK, Heagle AB, Penczek P, Grassucci RA, Frank J (1999) EF-G-dependent GTP hydrolysis induces translocation accompanied by large conformational changes in the 70S ribosome. *Nat Struct Biol* 6:643–647.
21. Agrawal RK, Penczek P, Grassucci RA, Frank J (1998) Visualization of elongation factor G on the *Escherichia coli* 70S ribosome: The mechanism of translocation. *Proc Natl Acad Sci USA* 95:6134–6138.
22. Frank J, Agrawal RK (2000) A ratchet-like inter-subunit reorganization of the ribosome during translocation. *Nature* 406:318–322.
23. Frank J, Gao H, Sengupta J, Gao N, Taylor DJ (2007) The process of mRNA-tRNA translocation. *Proc Natl Acad Sci USA* 104:19671–19678.
24. Valle M, *et al.* (2003) Locking and unlocking of ribosomal motions. *Cell* 114:123–134.
25. Stark H, Rodnina MV, Wieden HJ, van Heel M, Wintermeyer W (2000) Large-scale movement of elongation factor G and extensive conformational change of the ribosome during translocation. *Cell* 100:301–309.
26. Savelsbergh A, *et al.* (2003) An elongation factor G-induced ribosome rearrangement precedes tRNA-mRNA translocation. *Mol Cell* 11:1517–1523.
27. Savelsbergh A, Mohr D, Kothe U, Wintermeyer W, Rodnina MV (2005) Control of phosphate release from elongation factor G by ribosomal protein L7/12. *EMBO J* 24:4316–4323.
28. Peske F, Savelsbergh A, Katunin VI, Rodnina MV, Wintermeyer W (2004) Conformational changes of the small ribosomal subunit during elongation factor G-dependent tRNA-mRNA translocation. *J Mol Biol* 343:1183–1194.
29. Wintermeyer W, *et al.* (2004) Mechanisms of elongation on the ribosome: Dynamics of a macromolecular machine. *Biochem Soc Trans* 32:733–737.
30. Taylor DJ, *et al.* (2007) Structures of modified eEF2 80S ribosome complexes reveal the role of GTP hydrolysis in translocation. *EMBO J* 26:2421–2431.
31. Horan LH, Noller HN (2007) Intersubunit movement is required for ribosomal translocation. *Proc Natl Acad Sci USA* 104:4881–4885.
32. Yusupov MM, *et al.* (2001) Crystal structure of the ribosome at 5.5 A resolution. *Science* 292:883–896.
33. Rodnina MV, Savelsbergh A, Katunin VI, Wintermeyer W (1997) Hydrolysis of GTP by elongation factor G drives tRNA movement on the ribosome. *Nature* 385:37–41.
34. Dorner S, Brunelle JL, Sharma D, Green R (2006) The hybrid state of tRNA binding is an authentic translation elongation intermediate. *Nat Struct Mol Biol* 13:234–241.
35. Otwinowski Z, Minor W (1997) Processing of X-ray Diffraction Data Collected in Oscillation Mode. *Methods Enzymol Macromol Crystallogr* 276:307–326.
36. Collaborative Computational Project, N (1994) The CCP4 Suite: Programs for Protein Crystallography. *Acta Crystallogr D*:760–763.
37. Sheldrick GM (2008) A short history of SHELX. *Acta Crystallogr A*:112–122.
38. Terwilliger TC, Berendzen J (1999) Automated MAD and MIR structure solution. *Acta Crystallogr D* 55:849–861.
39. Murshudov GN, Vagin AA, Dodson EJ (1997) Refinement of macromolecular structures by the maximum-likelihood method. *Acta Crystallogr D* 53:240–255.
40. DeLano WL (2002) *The PyMol Molecular Graphics System* (DeLano Scientific, Palo Alto, CA).
41. Fabiola F, Korostelev A, Chapman MS (2006) Bias in cross-validated free R factors: Mitigation of the effects of non-crystallographic symmetry. *Acta Crystallogr D* 62:227–238.
42. Cate JH, Yusupov MM, Yusupova GZ, Earnest TN, Noller HF (1999) X-ray crystal structures of 70S ribosome functional complexes. *Science* 285:2095–2104.